Chinese Journal of Electronics
Vol.32, No.5, Sept. 2023

Optimization on the Dynamic Train Coupling Process in High-Speed Railway

CHENG Fanglin[1,2], TANG Tao[1,2], SU Shuai[1,2], and MENG Jun[3]

(1. *State Key Laboratory of Traffic Control and Safety, Beijing Jiaotong University, Beijing 100044, China*)

(2. *Frontiers Science Center for Smart High-speed Railway System, Beijing Jiaotong University, Beijing 100044, China*)

(3. *China Academy of Railway Science, Beijing 100044, China*)

Abstract — This work focuses on the driving strategy optimization problem of a scenario in which two trains come from two branches under virtual coupling, aiming at going through the junction area efficiently. A distance-discrete optimal control model is constructed. The optimization objective is to maximize the trip time during which the two trains operate in coupled state. The line conditions, dynamic properties of the trains and the safety protection constraints are considered. The nonlinear constraints are converted into linear constraints with piecewise affine function and logical variables, and the proposed problem is converted into mixed integer linear programming (MILP) problem which can be solved by existing solvers such as Cplex. Four simulation experiments are conducted to verify the effectiveness of MILP. The dynamic programming (DP) algorithm is used as the benchmark algorithm in the case study. Compared with DP algorithm in small state space, MILP has better performance since it shortens the coupling time. Moreover, the improvement of line capacity of virtual coupling is 35.42% compared with the fixed blocking system.

Key words — Virtual coupling, Junction area, Mixed integer linear programming (MILP).

I. Introduction

The demand for capacity of the railway is increasing rapidly in recent years, leading to the near-saturation of the existing network. Consequently, the infrastructure managers have being challenged to expand the capacity of the existing networks [1]. However, the improvement of the infrastructures meets with high difficulties due to the expensive costs. Therefore, the exploration of the next generation signalling, such as virtual coupling, attracts more attentions from the scholars.

Virtual coupling is a revolutionary innovation in railways because the physical connections between successive trains are removed and vehicle-to-vehicle (V2V) communication technology is implemented to realize the cooperative operation of multiple trains running in a small headway. In this article, the virtual coupling is based on the European Train Control System Level 3 (ETCS-3) plus an additional V2V communication layer in which trains exchange information about their kinematic parameters (i.e., speed, position, and acceleration). Five operational states (i.e., the ETCS-3 Running, Coupling, Coupled running, Unintentional decoupling, and Intentional decoupling) and their transitions for virtual coupling are defined in article [2]. The coupling process (i.e., the transition among ETCS-3 Running, Coupling, and Coupled running) for the two trains in the junction area is focused on in this paper. The main contributions are summarized as follows.

1) This article proposes a discrete model with distance as independent variable for train trajectory optimization in junction area. The line conditions (including running resistance and speed limits) and train characteristics are considered in the model. Moreover, the safety constraints caused by the switch are emphasized in this article.

2) Mixed integer linear programming (MILP) algorithm is used to solve the proposed model. Dynamic programming (DP) is used as a benchmark approach. DP and MILP are used in the virtual coupling control firstly. Compared with DP algorithm for small state space, the driving strategies solved by MILP shorten

Manuscript Received July 2, 2022; Accepted Dec. 3, 2022. This work was supported by the Talent Fund of Beijing Jiaotong University (2021RC271), the National Natural Science Foundation of China (52172322, U22A2046), the Foundation of China State Railway Group Co., Ltd. (L2021G003, L2022G010), the Beijing Natural Science Foundation (L201004, L191015), and the State Key Laboratory of Rail Traffic Control and Safety (RCS2022ZZ003, RCS2022ZI002).

 DOI:10.23919/cje.2022.00.189

the coupling time.

3) The capacity improvement rate of virtual coupling signaling concept is discussed compared with fixed blocking signaling concept. The results show that the average capacity improving rate is 35.42%.

The rest of the article is organized as follows. A literature review is presented in Section II. A specific problem description is developed in Section III. A coupling model is described in Section IV. Some cases are conducted to show the effectiveness of the proposed approach in Section V. Conclusions are presented in Section VI.

II. Literature Review

In earlier studies, the idea of virtually coupled train formations (VCTF) using independent train modules was discussed [3]. A prototype of the virtually coupled train (VCT) system was designed. The system included dispatching, control, communication, etc. The functionality was demonstrated through simulations [4].

In recent years, virtual coupling technology has made a series of progress with the promotion of the Shift2Rail project. In the virtual coupling control area, the capacity improvement via virtual coupling was discussed by giving a detailed virtual coupling process, which included various operational states and their transitions [2]. A multi-agent-system-based coordinated control model was proposed which could achieve real-time dynamic adjustment and ensure both the operation efficiency and safety in the high-speed railway [5]. Then, based on the control system, an intelligent dispatching system was proposed to improve the transportation capacity in railway stations [6]. The decentralized model predictive control (MPC) framework was applied to the leading and following trains in a convoy running. The simulation results demonstrated better performance and benefits of this new concept compared with the moving block system [7]. Besides, a cruising control approach for VCT on the basis of MPC was proposed [8]. A coasting control strategy was developed to improve the output of the MPC controller [9]. The coupling, keeping, and separation of virtual coupling were focused on. The position error correction was further considered aiming at reducing the gap control perturbations, and a robust gap controller was proposed [10]. Full supervision plus virtual coupling operating mode was developed within the European Rail Traffic Management system. The impact on communication links caused by time-varying delays was considered, and a coupling controller based on numerical analysis methodology was designed to account for this problem [11]. A method for the calculation of speed limit curve based on relative braking distance was put forward to ensure the following train keeping a safe distance from the leading train [12]. An analytic optimal control method for VCT was proposed as well as an algorithm based on Pontryagin's maximum principle was developed to solve the optimal control problem [13]. A controller based on generalized predictive control (GPC) and mixed artificial potential field (APF) was used to perform cooperative control and prevent collision of the virtual coupling train [14]. Similar study can be found in [15]–[18].

Previous studies are based on the straight line. The coupling process for the two trains in the junction area is focused on in this paper.

III. Problem Description

In this article, the optimization of coupling process for train control in the junction area is studied. The whole coupling process is shown in Fig.1.

In the ETCS-3 Running state, train A and train B are on different branch lines, respectively, which is shown in Fig.1, where V2I is a vehicle-to-infrastructure communication technology. s^A_{ini} and s^B_{ini} are the initial positions of train A and train B. s^P represents the position of switch, and the terminal position of train B is denoted as s^B_{end}. The coupling process of the two trains begins when train A goes through the switch firstly. Then, train B catches up with train A and couples with train A. The time-position curves of the two trains for the coupling process is shown in Fig.2.

In Fig.2, T_P is the total time spent in turning the switch (i.e., the trip time consumed by train A to pass the switch plus the transition time of the switch) to the right position for train B. The moving authority (MA) of train B is updated when the switch turns to the right position and is locked. T is the total running time for the two trains. In the ETCS-3 Running state, the switch is not in the right position, the end of MA under virtual coupling (EoA_{vc}) is on the switch, and the velocity at the EoA_{vc} is zero. In the Coupling state, the switch is in the right position, the EoA_{vc} represents the tail of train A plus safety margin (sm), and the velocity at the EoA_{vc} is V^A. In the Coupled running state, the relative distance between the two trains is the length of train A and sm, which is set to compensate for the impact of other unknown factors including the measurement error of train position and irregular track friction force [19].

On the premise of pre-calculating the speed profile of train A, the aim of this article is to figure out the optimal driving strategy for train B which minimizing the coupling time and maximizing the coupling efficiency. Because of the fixed total running time, the coupling

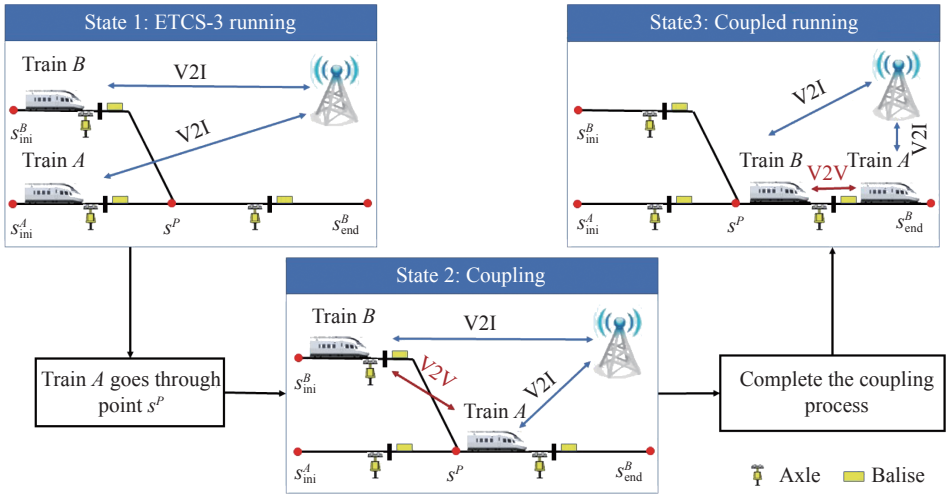

Fig. 1. Coupling process.

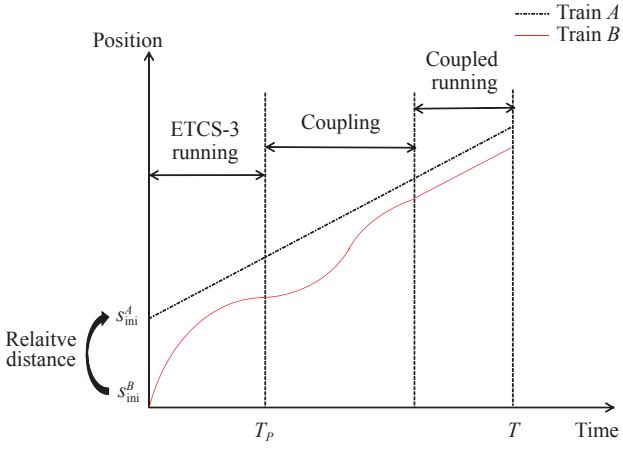

Fig. 2. The time-position curves of the two trains for the coupling process.

time will be decreased if the coupled time grows. Considering the complexity of the model, the objective of the model is to maximize coupled time.

IV. Model Formulation

In order to simplify the consideration of additional resistance, train position s is chosen as independent variable referring to previous works [20]–[22]. The constraints for this problem include basic resistance, additional resistance, speed limit, boundary conditions, maximum traction, and safety protection constraints.

In this section, the route of train B is split into N intervals to get a discrete-space model according to different gradients and the radius of the curve. The control regime of train B in each interval is uniform acceleration which can simplify the problem. Instead of using the velocity as the state, the kinetic energy is used for linearization.

The time that two trains in the coupled state is regarded as optimization objective, which is formulated as follows:

$$\max \text{ obj} = \sum_{k=1}^{N} t_{\text{coupled}}(k) \tag{1}$$

where $t_{\text{coupled}}(k)$ represents the coupled time in kth interval. The detailed calculation equation is shown in the end of this section.

In this article, a mass-point model is used like previous work in the train optimal control area [23]. The position of the mass-point represents the front of the train. The motion of train B is described by the following equation:

$$E^B(k+1) - E^B(k) = m^B a^B(k) l_k, \quad k = 1, 2, \ldots, N \tag{2}$$

where $E^B(k)$ is the kinetic energy of train B entering the kth interval and $E^B(k+1)$ is the kinetic energy of train B leaving the kth interval and entering the $(k+1)$th interval; l_k denotes the length of the kth interval; the mass of train B is denoted as m^B; the calculation formula of $m^B a^B(k)$ is as follows:

$$m^B a^B(k) = F^B(k) + R_b^B(E^B(k)) + R_k^B, \quad k = 1, 2, \ldots, N \tag{3}$$

where $F^B(k)$ denotes the control force in the kth interval; $R_b^B(E^B(k))$ and R_k^B represent the running resistance and additional resistance of train B in the kth interval respectively. $R_b^B(E^B(k))$ can be calculated as the following equation:

$$R_b^B(E^B(k)) = m^B c_1^B + 2c_2^B E^B(k), \quad k = 1, 2, \ldots, N \tag{4}$$

where c_1^B and c_2^B are related on the dynamic properties of train B; R_k^B is developed as follows:

$$R_k^B = m^B g \times \sin\varphi_k + R^B(r_k), \quad k = 1, 2, \ldots, N \tag{5}$$

where the gradient in the kth interval is denoted as φ_k and g represents the gravitational acceleration; r_k represents the curve radius in the kth interval; the curve resistance in the kth interval is denoted by $R^B(r_k)$, and it can be constructed as

$$R^B(r_k) = \begin{cases} \dfrac{6.30m^B}{r_k - 55}, & r_k \geq 300 \text{ (m)} \\ \dfrac{4.91m^B}{r_k - 30}, & r_k < 300 \text{ (m)} \end{cases}, \quad k = 1, 2, ..., N \tag{6}$$

Referring to trapezoidal integration rule [24], the time equation can be described as

$$t^B(k+1) = t^B(k) + \frac{1}{2}\left[\frac{1}{\sqrt{\dfrac{2E^B(k)}{m^B}}} + \frac{1}{\sqrt{\dfrac{2E^B(k+1)}{m^B}}}\right] l_k, \quad k = 1, 2, \ldots, N \tag{7}$$

where $t^B(k)$ is the time when train B enters the kth interval.

The traction or braking force is restricted by the maximum traction force $F^B_{\max}(E^B(k))$ and maximum braking force $F^B_{\min}$. The constraint can be calculated as follows.

$$F^B_{\min} \leq F^B(k) \leq F^B_{\max}(E^B(k)), \quad k = 1, 2, \ldots, N \tag{8}$$

where $F^B_{\min}$ is considered as a constant in this article. Maximum traction force $F^B_{\max}(E^B(k))$ is relative to the kinetic energy. The equation of the maximum traction force is shown as

$$F^B_{\max}(E^B(k)) = \begin{cases} c_a^B, & E^B(k) \leq E_c \\ c_3^B + c_4^B\sqrt{\dfrac{2E^B(k)}{m^B}} + c_5^B\dfrac{2E^B(k)}{m^B}, & \text{otherwise} \end{cases}, \quad k = 1, 2, \ldots, N \tag{9}$$

where c_a^B, c_3^B, c_4^B, c_5^B, and E_c depend on train characteristic.

Besides, speed limit is also a significant constraint for train operation. Speed limit can be described as

$$\epsilon \leq E^B(k) \leq E_k, \quad k = 1, 2, \ldots, N+1 \tag{10}$$

where E_k represents the limited kinetic energy in the kth interval; ϵ is a small positive number.

There are also some boundary conditions. In this paper, the initial kinetic energy of train B is fixed. The running time T is determined by train A.

$$\begin{cases} 1\text{: } E^B(1) = E^B_{\text{ini}} \\ 2\text{: } E^B(N+1) = E^B_{\text{end}} \\ 3\text{: } t^B(1) = 0 \\ 4\text{: } t^B(N+1) = T \\ 5\text{: } s_1^B = 0 \\ 6\text{: } s_{N+1}^B = L \end{cases} \tag{11}$$

where E^B_{ini} denotes the initial kinetic energy of train B; E^B_{end} denotes the terminal kinetic energy of train B and is the same as the kinetic energy of train A since the two trains are in coupled state when they come to the journey's end; $t^B(1)$ and $t^B(N+1)$ represent the initial time and the terminal time for train B respectively; s_1^B and s_{N+1}^B represent the initial position and the terminal position for train B respectively; T is the running time; L is the length of the line.

The movement of train B can be divided into two situations, i.e., train B is allowed to go through the switch and cannot go through the switch. The first situation happens when train A has not gone through the switch or the state of the switch is improper. In this situation, train B needs to stop before it reaches the switch. The second situation happens when train A has gone through the switch and the state of the switch is proper. In this situation, the two trains must keep relative braking distance. The protection mechanisms of the two situations can be described as

$$\begin{cases} 1\text{: } t^B(k) \leq T_P \leftrightarrow \delta_{1,1}(k) = 1 \\ 2\text{: } E^B_{\max,k} + M(1 - \delta_{1,1}(k)) \geq E^B(k) \\ 3\text{: } s_k \leq s^A_{t^B(k)} - L^A - \text{sm} - \text{rbs}(k) + M\delta_{1,1}(k) \end{cases} \quad \text{where } k = 1, 2, \ldots, N+1 \tag{12}$$

where $t^B(k)$ represents the current time; T_P represents the time that the MA of train B changes; $E^B_{\max,k}$ represents the maximum kinetic energy in which the train B applies the brake using the maximum braking force at the beginning position of the kth interval, just in time to stop at the switch; s^P is the switch position; L^A is the length of train A; sm is the small margin; $\text{rbs}(k)$ represents the relative braking distance; $\delta_{1,1}(k)$ is a binary variable. The calculation of $\text{rbs}(k)$ is as follows:

$$\text{rbs}(k) = \begin{cases} E^B(k) & \leq E^A_{t^B(k)} \\ \dfrac{(E^A_{t^B(k)} - E^B(k))}{F^B_{\min}} E^B(k) & > E^A_{t^B(k)} \end{cases} \tag{13}$$

where $E^A_{t^B(k)}$ represents the kinetic energy of train A at the current time $t^B(k)$.

The judgement condition for Coupled running is described as follows:

$$\begin{cases} 1{:}\ E^A_{t^B(k)} - \eta_e \le E^B(k) \leftrightarrow \delta_{1,2}(k) = 1 \\ 2{:}\ E^B(k) \le E^A_{t^B(k)} \leftrightarrow \delta_{1,3}(k) = 1 \\ 3{:}\ \delta_{1,6}(k) = \delta_{1,2}(k)\delta_{1,3}(k) \\ 4{:}\ s^A_{t^B(k)} - L^A - \mathrm{sm} - s_{\mathrm{ths}} \le s_k \leftrightarrow \delta_{1,4}(k) = 1 \\ 5{:}\ s_k \le s^A_{t^B(k)} - L^A - sm \leftrightarrow \delta_{1,5}(k) = 1 \\ 6{:}\ \delta_{1,7}(k) = \delta_{1,4}(k)\delta_{1,5}(k) \\ 7{:}\ \delta(k) = \delta_{1,6}(k)\delta_{1,7}(k) \\ \qquad \text{where } k = 1, 2, \ldots, N+1 \end{cases} \tag{14}$$

where $\delta(k) = 1$ represents that train A and train B are in coupled state when train B enters the kth interval, otherwise, $\delta(k) = 0$. The first three constraints 1–3 is the kinetic energy range for Coupled running. The next three constraints 4–6 is the position range for Coupled running. E_{ths} is the kinetic energy threshold for unintentional decoupling [2]; s_{ths} is the distance threshold for unintentional decoupling [2]. $\delta_{1,i}(k)$ $(i = 2, 3, \ldots, 7)$ is a binary variable.

The logical variable $\delta(k) \in \{0, 1\}$ is introduced to calculate $t_{\mathrm{coupled}}(k)$, the detailed calculation of $t_{\mathrm{coupled}}(k)$ is as follows:

$$t_{\mathrm{coupled}}(k-1) = \delta(k-1)\delta(k)(t(k) - t(k-1)), \quad k = 2, 3, \ldots, N+1 \tag{15}$$

The equation (15) shows that the judgement condition for the coupled state in the $(k-1)$th interval. The judgement condition is that the two trains enter and leave the $(k-1)$th interval in coupled state.

Now, a discrete model has been established. There are still some nonlinear constraints. Therefore, logical variable and piecewise affine (PWA) are imported for non-linear conditions (e.g., equations (7) and (9)). The principle of PWA approximation is shown in Fig.3. The black solid line is the original function, the red-dashed line is the PWA approximation. The linearized results for (7) and (9) are shown in Appendix A. The linearized results for (15) shown in Appendix B. Then, the linearized model can be solved by the existing solvers (e.g., Cplex).

V. Case Study

In this section, some numerical experiments in which train A and train B are on the different branch lines are conducted. DP algorithm is used as benchmark algorithm since it is an effective method for the multi-decision problem [25]. Matlab 2018 is used to implement DP algorithm. MILP method is compared with DP algorithm, the implementation of MILP method is based on Matlab 2018 + Yalmip + Cplex 12.8. To simplify the consideration, the motion of train A is an uniform motion whose motion sequence has been pre-calculated. The motion sequence of train B is calculated by DP and MILP. Besides, it is assumed that train A and train B have the same braking characteristic and the same mass.

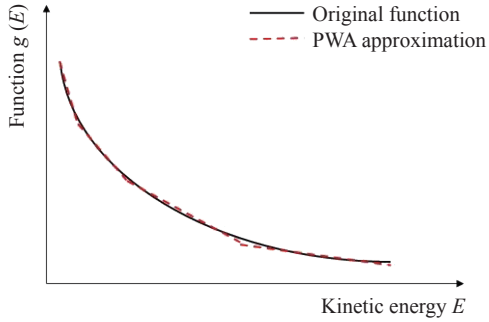

Fig. 3. The PWA approximation of the nonlinear function.

The parameters of the line and trains are shown in Table 1. To simplify the discussion, the distance is equally divided into N intervals. The parameters of PWA are shown in Table 2. Four cases are conducted in the case study.

Table 1. Parameters of line and trains

Property	Symbol	Value
The total length of the interval (m)	–	28000
Switch position (m)	s^P	5000
The time for switch move (s)	t_P	10
Gradient	r	−1
Train mass (kg)	m	1×10^5
Resistance coefficient 1	c_1^B	0.02
Resistance coefficient 2	c_2^B	4.42×10^5
Train length (m)	L^A, L^B	200
Interval length (m)	l_k	350
Safety margin (m)	sm	500
Maximum energy (J)	$E_{\max}$	4000
Minimum energy (J)	ϵ	0.1
Maximum braking deceleration (N)	$F^B_{\min}$	1×10^5
Kinetic energy threshold (J)	E_{ths}	6
Distance threshold (m)	s_{ths}	10
Velocity step for DP (m)	–	0.05
Time step for DP (small state space)	–	0.05
Time step for DP (large state space)	–	0.025
Distance step for DP	–	350

1) In the first case, the impact of different initial velocities of train B is discussed. The velocity, position, and time are considered as the state of train B. The acceleration and deceleration are defined as action. The coupled time is defined as reward. The results of DP and MILP with the same initial position and different initial velocities are shown Table 3. The initial position of train A is s^A_{ini}, the initial position of train B is s^B_{ini}, the initial velocity of train A is v^A_{ini}, the initial velocity of train B is v^B_{ini}. MILP has better performance since it

Table 2. The Parameters of PWA

Segment n	α_n	β_n	E (J)
1	-0.0141	1.0246	0–71.5
2	-1.6134×10^{-5}	0.0249	71.5–850
3	-2.9479×10^{-6}	0.0136	850–2000
4	-1.1622×10^{-5}	0.0009	2000–4000
5	0	0.7472	0–180
6	-0.0003	0.7919	180–660
7	-7.9153×10^{-5}	0.6435	660–4000

has shorter coupling time. The coupling time solved by MILP reduced by 3.99% compare with DP in small state space. The reason for this phenomenon is that the time state and velocity state are continuous in MILP, whereas, the states are discrete in DP. The solution of DP with more refined state is closer to MILP (i.e., the time step is 0.025 s in large state space, whereas, the time step is 0.05 s in small state space). Although there are numerical differences between the two methods, the same trends are existed in both methods. The coupling time decreases firstly and then flattens out, because of the turning process of the switch and passing sequences of the trains (i.e., train A passes the switch firstly, then, the switch is turned into the proper state, train B passes the switch secondly). When the T_P is fixed, the higher the initial velocity brings the longer decelerate distance to prevent train B from triggering the safety protection mechanism. The effect of the initial velocity is offset by deceleration, which is shown in Fig.4.

Table 3. The coupling time solved by DP with different state spaces and MILP under different initial conditions

Initial conditions ($s^A_{\text{ini}} = 3000$ m, $s^B_{\text{ini}} = 0$ m, $v^A_{\text{ini}} = 60$ m/s)	Coupling time		
	MILP	DP (small state space)	DP (large state space)
$v^B_{\text{ini}} = 50$ m/s	341.53 s	358.45 s	340.98 s
$v^B_{\text{ini}} = 55$ m/s	341.55 s	358.45 s	340.98 s
$v^B_{\text{ini}} = 60$ m/s	338.65 s	352.60 s	340.93 s
$v^B_{\text{ini}} = 65$ m/s	336.70 s	352.60 s	335.15 s
$v^B_{\text{ini}} = 70$ m/s	336.29 s	352.60 s	335.15 s
$v^B_{\text{ini}} = 75$ m/s	336.10 s	352.60 s	335.15 s
$v^B_{ini} = 80$ m/s	336.26 s	346.80 s	335.13 s
$v^B_{\text{ini}} = 85$ m/s	335.17 s	341.00 s	329.33 s

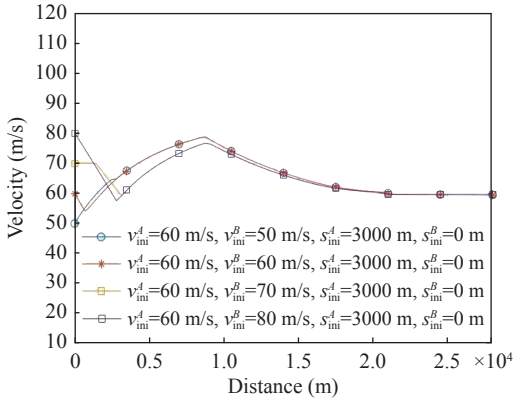

Fig. 4. The velocity-distance curve of train B with fixed initial velocities solved by MILP.

2) In the second case, the impact of different initial positions of train B is discussed. Only MILP algorithm is discussed in this case due to the better performance of MILP. According to the results in Table 4, the initial velocities of the two trains are fixed. The initial position of train A is closer to the switch. The detailed velocity-distance curve of train B is shown in Fig.5. With the decrease of the distance between train A and the switch, train A goes through the switch earlier, therefore, T_p is smaller, and then train B do not need to prevent triggering the safety protection mechanism by deceleration.

Table 4. The coupling time solved by MILP under fixed initial velocities and different initial positions

Initial velocity $v^A_{\text{ini}}, v^B_{\text{ini}}$	Coupling time		
	Initial position $s^A_{\text{ini}} = 3000$ m, $s^B_{\text{ini}} = 0$ m	Initial position $s^A_{\text{ini}} = 3500$ m, $s^B_{\text{ini}} = 0$ m	Initial position $s^A_{\text{ini}} = 4000$ m, $s^B_{\text{ini}} = 0$ m
$v^A_{\text{ini}} = 60$ m/s, $v^B_{\text{ini}} = 50$ m/s	341.53 s	368.17 s	412.12 s
$v^A_{\text{ini}} = 60$ m/s, $v^B_{\text{ini}} = 55$ m/s	341.55 s	344.85 s	383.05 s
$v^A_{\text{ini}} = 60$ m/s, $v^B_{\text{ini}} = 60$ m/s	338.65 s	345.04 s	359.75 s

3) In the third case, the effectiveness of the constraints is tested, and a velocity protection surface is calculated by (12). The velocity-distance curve of train B under certain initial condition (i.e., $v^A_{\text{ini}} = 60$ m/s, $v^B_{\text{ini}} = 60$ m/s, $s^A_{\text{ini}} = 3000$ m, $s^B_{\text{ini}} = 0$ m) and the correspond velocity protection surface is shown in Fig.6. The velocity protection surface is divided into two parts. The first part is corresponding to situation one. In this situation, train B must stop before it reaches the switch. The red solid line is the EoA_{vc} before T_P. The

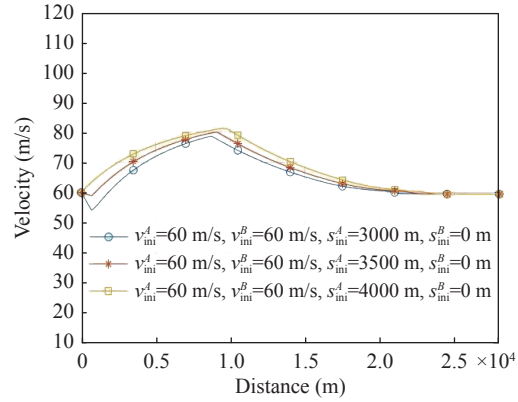

Fig. 5. The velocity-distance curve of train B with different initial positions solved by MILP.

second part is corresponding to situation two. In this situation, the two trains keep relative braking distance. The black dash line is the $\mathrm{EoA}_{\mathrm{vc}}$ after T_P. The velocity-distance curve of train B satisfies the protection mechanism (i.e., equation (12)). The separation between the two trains is shown in Fig.7. The black solid line is T_P. It is shown that the separation decreases and is gradually stable at the preset sm after T_P.

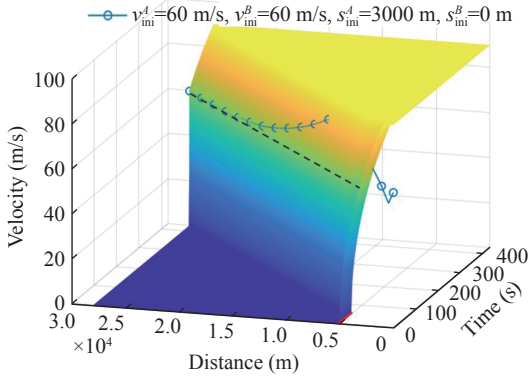

Fig. 6. The velocity protection surface of train B and the velocity-distance curve of train B solved by MILP under fixed situation.

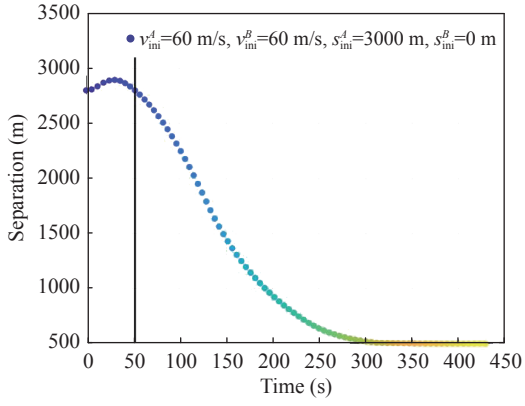

Fig. 7. The separation of the two trains under fixed initial condition.

4) In the fourth case, the improvement of the line capacity in the junction area is discussed by calculating the reciprocal of the headway on the switch. The improvement rates of line capacity with virtual coupling compared with fixed block are shown in Fig.8. There are four classes for comprehensive discussion. The four classes include different initial velocities and different initial positions. In each class, different initial velocitiesis are set for train B to discuss the improvement rate. In each condition, virtual coupling has better performance than fixed block. The results show that the average capacity improving rate of the four classes is 35.42%. The average improvement rates in the four classes are shown in Table. 5. It has been calculated that the essentially difference in four classes of initial conditions is T_P since it is the switching point for the two protections. The different T_P corresponding to the four classes are shown in Table. 5. A larger value of T_P brings greater improvement. The possible reason for this phenomenon is that the different speed limits with the two signal concepts. If T_P is larger, the relative distance between train A and train B is shorter since train B have more time to shorten the relative distance, and hence, virtual coupling has better performance in this situation. The velocity-distance curve of train B is shown in Fig.9 with different signaling concepts. The reason that the line capacity is improved is that the higher average velocity in virtual coupling.

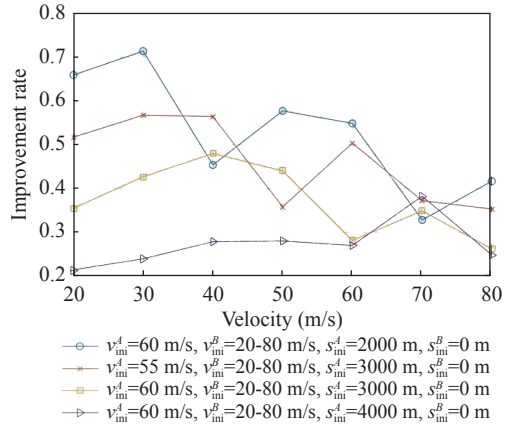

Fig. 8. The improvement rate of line capacity with virtual coupling compared with fixed block under different initial condition.

VI. Conclusions

In this article, a coupling linear model is constructed for the two trains in the junction area. Serval cases with different initial conditions are conducted to verify the effectiveness of the proposed model. MILP approach is compared with DP algorithm in the case

Table 5. The investigation for the improvement of line capacity with virtual coupling compared with fixed block

Different initial conditions	T_P	Average improvement rate
$s_{\text{ini}}^A = 4000$ m, $v_{\text{ini}}^A = 60$ m/s, $s_{\text{ini}}^B = 0$ m, $v_{\text{ini}}^B = 20$–80 m/s	26.67 s	24.45%
$s_{\text{ini}}^A = 3000$ m, $v_{\text{ini}}^A = 60$ m/s, $s_{\text{ini}}^B = 0$ m, $v_{\text{ini}}^B = 20$–80 m/s	43.33 s	32.33%
$s_{\text{ini}}^A = 3000$ m, $v_{\text{ini}}^A = 55$ m/s, $s_{\text{ini}}^B = 0$ m, $v_{\text{ini}}^B = 20$–80 m/s	46.36 s	40.43%
$s_{\text{ini}}^A = 2000$ m, $v_{\text{ini}}^A = 60$ m/s, $s_{\text{ini}}^B = 0$ m, $v_{\text{ini}}^B = 20$–80 m/s	60.00 s	44.48%

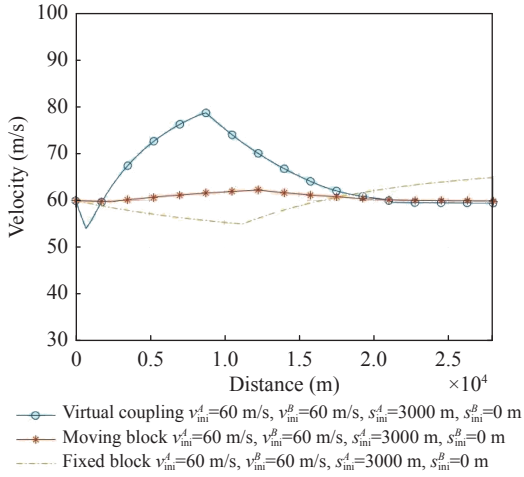

Fig. 9. The velocity-distance curve of train B with different signaling concepts.

study. The results solved by MILP has better performance since it has shorter coupling time compared with DP algorithm in small state space. Meanwhile, with the increase of the train B's initial velocity, the coupling time decreases firstly and then levels off. Besides, with the increase of the relative initial distance between the two trains, it takes longer time for train B to couple with train A. Moreover, compared with other signaling concepts, the line capacity is significantly improved with virtual coupling.

Appendix A

The nonlinear item of (7) is $g(k) = 1/(2\sqrt{2E^B(k)/m^B})$. The linearization for nonlinear (7) is as follows:

$$t^B(k+1) = t^B(k) + (g(k) + g(k+1))l_k, \quad k = 1, 2, ..., N+1 \tag{A-1}$$

$$\begin{aligned} g(k) =& [\alpha_1 \quad \alpha_2 \quad \alpha_3 \quad \alpha_4] \times [z_1(k) \quad z_2(k) \quad z_3(k) \quad z_4(k)]^{\mathrm{T}} \\ &+ [\delta_1(k) \quad \delta_2(k) - \delta_5(k) \quad \delta_3(k) - \delta_6(k) \quad \delta_4(k) - \delta_7(k)] \\ &\times [\beta_1 \quad \beta_2 \quad \beta_3 \quad \beta_4]^{\mathrm{T}} - \alpha_2 z_5(k) - \alpha_3 z_6(k) - \alpha_4 z_7(k), \\ & E^B(k) \le E_i \leftrightarrow \delta_i(k) = 1, \\ & \delta_{j+4}(k) = \delta_j(k)\delta_{j+1}(k), \\ & z_i(k) = \delta_i(k)E(k), \\ & z_{j+4}(k) = \delta_1(k)z_{j+1}(k), \\ & i = 1, 2, 3, 4, \quad j = 1, 2, 3, \quad k = 1, 2, \ldots, N+1 \end{aligned} \tag{A-2}$$

where $\delta_i \in \{0, 1\}$ and $\delta_j \in \{0, 1\}$ are binary variable.

The linearization for nonlinear (9) is as follows:

$$\begin{aligned} F_{\max}^B(k) =& [-\alpha_7 \quad \alpha_6 - \alpha_7 \quad \alpha_5 - \alpha_6 + \alpha_7] \\ &\times [z_8(k) \quad z_9(k) \quad z_{10}(k)]^T \\ &+ [-\beta_7 \quad \beta_6 - \beta_7 \quad \beta_5 - \beta_6 + \beta_7] \\ &\times [\delta_8(k) \quad \delta_9(k) \quad \delta_{10}(k)]^{\mathrm{T}} \\ &+ \alpha_7 E^B(k) + \beta_7, \\ & E^B(k) \le E_i \leftrightarrow \delta_{i+3}(k) = 1, \\ & \delta_{10}(k) = \delta_8(k)\delta_9(k), \\ & z_j(k) = \delta_j(k)E^B(k), \\ & i = 5, 6, \quad j = 8, 9, 10, \quad k = 1, 2, \ldots, N+1 \end{aligned} \tag{A-3}$$

where $\delta_i \in \{0, 1\}$ and $\delta_j \in \{0, 1\}$ are binary variable.

Appendix B

The linearization for nonlinear (15) is as follows:

$$\begin{aligned} & \delta_{11}(k-1) = \delta(k)\delta(k-1), \\ & z_{11}^B(k) = t^B(k)\delta_{11}(k-1), \\ & z_{12}^B(k) = t^B(k-1)\delta_{11}(k-1), \\ & t_{\text{couple}}(k-1) = z_{11}^B(k) - z_{12}^B(k), \\ & k = 2, 3, \ldots, N+1 \end{aligned} \tag{B-1}$$

The nonlinear function caused by logical variables can be linearized by the three properties according to [26].

References

[1] J. Aoun, E. Quaglietta, and R. M. P. Goverde, "Investigating market potentials and operational scenarios of virtual coupling railway signaling," *Transportation Research Record:Journal of the Transportation Research Board*, vol.2674, no.8, pp.799–812, 2020.

[2] E. Quaglietta, M. Wang, and R. M. P. Goverde, "A multi-state train-following model for the analysis of virtual coupling railway operations," *Journal of Rail Transport Planning & Management*, vol.15, article no.100195, 2020.

[3] U. Bock and G. Bikker, "Design and development of a future freight train concept-"Virtually Coupled Train Formations"," *IFAC Proceedings Volumes*, vol.33, no.9, pp.395–400, 2000.

[4] S. Konig and E. Schnieder, "Modeling and simulation of an operation concept for future rail traffic," in *Proceedings of 2001 IEEE Intelligent Transportation Systems*, Oakland, CA, USA, pp.808–812, 2001.

[5] L. Liu, P. Wang, B. Zhang, *et al.*, "Coordinated control method of virtually coupled train formation based on multi agent system," in *Proceeding of the Second International Conference on Smart Vehicular Technology, Transportation, Communication and Applications*, Mount Emei,

China, pp.225–233, 2018.
[6] L. Liu, P. Wang, W. Wei, *et al.*, "Intelligent dispatching and coordinated control method at railway stations for virtually coupled train sets," in *Proceeding of 2019 IEEE Intelligent Transportation Systems Conference*, Auckland, New Zealand, pp.607–612, 2019.
[7] J. Felez, Y. Kim, and F. Borrelli, "A model predictive control approach for virtual coupling in railways," *IEEE Transactions on Intelligent Transportation Systems*, vol.20, no.7, pp.2728–2739, 2019.
[8] J. F. She, K. C. Li, L. Yuan, *et al.*, "Cruising control approach for virtually coupled train set based on model predictive control," in *Proceeding of the 23rd International Conference on Intelligent Transportation Systems*, Rhodes, Greece, pp.1–6, 2020.
[9] Z. Y. Wu, C. H. Gao, and T. Tang, "A virtually coupled metro train platoon control approach based on model predictive control," *IEEE Access*, vol.9, pp.56354–56363, 2021.
[10] J. Park, B. H. Lee, and Y. Eun, "Virtual coupling of railway vehicles: Gap reference for merge and separation, robust control, and position measurement," *IEEE Transactions on Intelligent Transportation Systems*, vol.23, no.2, pp.1085–1096, 2022.
[11] C. Di Meo, M. Di Vaio, F. Flammini, *et al.*, "ERTMS/ETCS virtual coupling: Proof of concept and numerical analysis," *IEEE Transactions on Intelligent Transportation Systems*, vol.21, no.6, pp.2545–2556, 2020.
[12] Z. D. Song, X. N. Xu, H. Li, *et al.*, "Study on virtual-coupling-orientated train control technique," *Railway Standard Design*, vol.63, no.6, pp.155–159, 2019. (in Chinese)
[13] Y. F. Liu, Y. Zhou, S. Su, *et al.*, "An analytical optimal control approach for virtually coupled high-speed trains with local and string stability," *Transportation Research Part C: Emerging Technologies*, vol.125, article no.102886, 2021.
[14] Y. Cao, J. K. Wen, and L. C. Ma, "Tracking and collision avoidance of virtual coupling train control system," *Future Generation Computer Systems*, vol.120, pp.76–90, 2021.
[15] W. T. Liu, S. Su, T. Tang, *et al.*, "A DQN-based intelligent control method for heavy haul trains on long steep downhill section," *Transportation Research Part C: Emerging Technologies*, vol.129, article no.103249, 2021.
[16] S. Su, X. K. Wang, Y. Cao, *et al.*, "An energy-efficient train operation approach by integrating the metro timetabling and eco-driving," *IEEE Transactions on Intelligent Transportation Systems*, vol.21, no.10, pp.4252–4268, 2020.
[17] Q. Wang, M. Chai, H. J. Liu, *et al.*, "Optimized control of virtual coupling at junctions: a cooperative game-based approach," *Actuators*, vol.10, no.9, article no.207, 2021.
[18] H. Zhao and X. W. Dai, "Event-triggered adaptive control for multiple high-speed trains with deception attacks in bottleneck sections," *Information Sciences*, vol.547, pp.470–481, 2021.
[19] Y. B. Zhao and P. Ioannou, "Positive train control with dynamic headway based on an active communication system," *IEEE Transactions on Intelligent Transportation Systems*, vol.16, no.6, pp.3095–3103, 2015.
[20] R. F. Liu and I. M. Golovitcher, "Energy-efficient operation of rail vehicles," *Transportation Research Part A: Policy and Practice*, vol.37, no.10, pp.917–932, 2003.
[21] S. Su, T. Tang, J. Xun, *et al.*, "Design of running grades for Energy-Efficient train regulation: A case study for Beijing Yizhuang Line," *IEEE Intelligent Transportation Systems Magazine*, vol.13, no.2, pp.189–200, 2021.
[22] B. Y. Su, T. Tang, S. Su, *et al.*, "Integrated rescheduling of train timetables and rolling stock circulation for metro line disturbance management: a Q-learning-based approach," *Engineering Optimization*, in press, 2023.
[23] R. Franke, M. Meyer, and P. Terwiesch, "Optimal control of the driving of trains," *Automatisierungstechnik*, vol.50, no.12, pp.606–614, 2002.
[24] Y. H. Wang, B. De Schutter, T. J. J. van den Boom, *et al.*, "Optimal trajectory planning for trains-A pseudospectral method and a mixed integer linear programming approach," *Transportation Research Part C: Emerging Technologies*, vol.29, pp.97–114, 2013.
[25] R. S. Sutton and A. G. Barto, *Reinforcement Learning: An Introduction*. MIT Press, Cambridge, MA, USA, pp. 73–88, 1998.
[26] H. Williams, "Model building in mathematical programming," *Mathematics and Computers in Simulation*, vol.33, no.1, pp.78–79, 1991.

CHENG Fanglin was born in 1996. She received the B.E. degree from Beijing Jiaotong University, Beijing, China in 2019. She received the M.E. degreee with the State Key Laboratory of Rail Traffic Control and Safety in Beijing Jiaotong University, Beijing, China, in 2022. Her current research interests include intelligent control, machine learning, and energy-efficient train operation in railway system. (Email: 19120200@bjtu.edu.cn)

TANG Tao was born in 1963. He received the Ph.D. degree in control theory from the Institute of Automation, Chinese Academy of Sciences, Beijing, China, in 1991. He is currently a Professor and the Director of the State Key Laboratory of Rail Traffic Control and Safety, Beijing Jiaotong University. His research interests include communication-based train control, high-speed train control system, and intelligent transportation systems. (Email: ttang@bjtu.edu.cn)

SU Shuai (corresponding author) was born in 1987. He received the Ph.D. degree from Beijing Jiaotong University, Beijing, China in 2016. He is currently working as the Deputy Director with the Frontiers Science Center for Smart High-Speed Railway System, Beijing Jiaotong University. His current research interests include energyefficient operation and control in railway systems, intelligent train control and dispatching. (Email: shuaisu@bjtu.edu.cn)

MENG Jun was born in 1983. He received the M.S. degree from Beijing Jiaotong University, Beijing, China, in 2018. Currently he works as an Associate Researcher in Signal & Communication Research Institute, China Academy of Railway Sciences Corporation Limited. His research interests include intelligent train control and information technology in railway system. (Email: mengjun1983@126.com)